J. Eukaryot. Microbiol., 56(4), 2009 pp. 373–384
© 2009 The Author(s)
Journal compilation © 2009 by the International Society of Protistologists
DOI: 10.1111/j.1550-7408.2009.00412.x

Light Microscopic Observations, Ultrastructure, and Molecular Phylogeny of *Hicanonectes teleskopos* n. g., n. sp., a Deep-Branching Relative of Diplomonads

JONG SOO PARK, MARTIN KOLISKO, AARON A. HEISS and ALASTAIR G.B. SIMPSON

Canadian Institute for Advanced Research, Program in Integrated Microbial Diversity, and Department of Biology, Dalhousie University, Halifax, B3H 4J1 Canada

ABSTRACT. We describe *Hicanonectes teleskopos* n. g., n. sp., a heterotrophic flagellate isolated from low-oxygen marine sediment. *Hicanonectes teleskopos* has a ventral groove and two unequal flagella, and rapidly rotates during swimming. At the ultrastructural level *H. teleskopos* is a ''typical excavate'': it displays flagellar vanes, a split right microtubular root, ''I,'' ''B,'' and ''C'' fibres, a singlet microtubular root, and a possible composite fibre. Small subunit rRNA (SSU rRNA) gene phylogenies and an ''arched'' B fibre demonstrate that *H. teleskopos* belongs to Fornicata (i.e. diplomonads, retortamonads, and relatives). It forms a clade with the deep-branching fornicate *Carpediemonas*, with moderate-to-strong bootstrap support, although their SSU rRNA gene sequences are quite dissimilar. *Hicanonectes* differs from *Carpediemonas* in cell shape, swimming behaviour, number of basal bodies (i.e. 4 vs. 3), number of flagellar vanes (i.e. 2 vs. 3), anterior root organization, and by having a cytopharynx. Like *Carpediemonas* and *Dysnectes*, *Hicanonectes* has conspicuous mitochondrion-like organelles that lack cristae and superficially resemble the hydrogenosomes of parabasalids, rather than the mitosomes of their closer relatives the diplomonads (e.g. *Giardia*).

Key Words. Anaerobe, basal eukaryote, excavate, *Giardia*, hydrogenosome, metamonad, microaerophile, protist, Protozoa.

FORNICATA is a recently established taxon within Excavata that houses diplomonads, retortamonads, *Carpediemonas*, and the newly described *Dysnectes* (Simpson 2003; Yubuki et al. 2007). Diplomonads are by far the best known of these groups, and include free-living, commensal, and parasitic species, for example, the well-studied human parasite *Giardia intestinalis*, also known as *Giardia lamblia* (Kulda and Nohýnková 1978). With one exception retortamonads are commensals or parasites, but have not been definitively connected to any human or livestock diseases (Kulda and Nohýnková 1978). *Carpediemonas* and *Dysnectes* are small, free-living, and slowly swimming biflagellated cells that inhabit oxygen-poor marine sediments (Ekebom, Patterson, and Vørs 1996; Lee and Patterson 2000; Simpson and Patterson 1999; Yubuki et al. 2007). There are just two nominal species of *Carpediemonas*, while *Dysnectes* is monospecific. Retortamonads, *Carpediemonas*, and *Dysnectes* have a ''typical excavate'' morphology, meaning that they possess a longitudinal feeding groove supported by a particular organization of cytoskeletal elements, and associated with a vane-bearing posterior flagellum (Simpson 2003; Yubuki et al. 2007). These three groups also display a unique organization of one cytoskeletal element, the B fibre/arched fibre, and this organization is the defining synapomorphy of Fornicata (Simpson 2003; Yubuki et al. 2007). The monophyly of Fornicata is well supported by small subunit ribosomal RNA (SSU rRNA) gene phylogenies (Keeling and Brugerolle 2006; Kolisko et al. 2008; Simpson 2003; Simpson et al. 2002b; Yubuki et al. 2007), and a *Carpediemonas*+diplomonads clade is recovered in protein phylogenies, in the absence of data from retortamonads and *Dysnectes* (Simpson, Inagaki, and Roger 2006; Simpson, MacQuarrie, and Roger 2002a; Simpson et al. 2002b). Small subunit rRNA gene trees indicate that diplomonads and retortamonads are specifically related, although a recent study recovers retortamonads as a paraphyletic group (Cepicka et al. 2008). *Carpediemonas* and *Dysnectes* are recovered as successive basal branches within Fornicata (Yubuki et al. 2007).

Fornicata is of great importance to researchers interested in eukaryotic cell evolution, for two main reasons: Firstly, molecular phylogenies that include diplomonads have tended to place them at or near the base of the eukaryotic tree (Ciccarelli et al. 2006; Hashimoto et al. 1994, 1995; Sogin et al. 1989); consequently diplomonads have often been considered to be relatively underived representatives of the first eukaryotic cell (e.g. Cavalier-Smith 1995). Secondly, these organisms do not possess classical mitochondria and were for a long time considered to be amitochondrial. However, genes of mitochondrial origin have been discovered in diplomonad nuclear genomes (Horner and Embley 2001; Roger et al. 1998; Tachezy, Sánchez, and Müller 2001) and extremely small ($\sim$ 50 nm across) remnant mitochondrial organelles, called mitosomes, have been identified in *G. intestinalis* (Tovar et al. 2003). The only known function of the *Giardia* mitosomes is iron–sulfur cluster assembly. In contrast to *Giardia*, *Carpediemonas membranifera* and *Dysnectes brevis* both possess rather large double membrane-bounded organelles with no cristae (Simpson and Patterson 1999; Yubuki et al. 2007). The larger biovolume of these organelles hints that they might be involved in more metabolic processes than the mitosomes of *Giardia*.

From a sample of low-oxygen marine sediment we encountered and cultured a biflagellated protist with a relatively inconspicuous longitudinal groove, which rotated during swimming and did not closely resemble any described organism that we were aware of. Surprisingly, ultrastructural study indicated that this organism is a ''typical excavate,'' and that it bears conspicuous mitochondrion-like organelles that lack cristae. Phylogenetic analyses of its SSU rRNA genes, and the presence of the proposed structural synapomorphy, demonstrate that the organism is a member of Fornicata. It is sufficiently distinct in ultrastructure and at the sequence level to merit description as a new taxon, *Hicanonectes teleskopos* n. g., n. sp.

MATERIALS AND METHODS

Isolation and culture. *Hicanonectes teleskopos* was isolated from anoxic marine intertidal sediments from a sheltered embayment on Salt Spring Island, BC, Canada (48°46′N, 123°28′W; sampled October 2007). Crude cultures were established by dispersing a sediment sample in TYSGM media (Diamond 1982), prepared without bovine serum, diluted 1:1 with sterile seawater, and supplemented with 30 ml horse serum/L. A xenic monoeukaryotic culture was established through one round of single cell isolation and several rapid transfers of the culture to fresh media. Cultures were maintained in this medium in 15 ml polypropylene tubes with 10–12 ml of media per tube. Cultures were grown at 21 °C and subculturing was performed every 4 d.

Light microscopy. Live *H. teleskopos* cells were observed with phase contrast microscopy using a Zeiss Axiovert 200 M mi-

Corresponding Author: A.G.B. Simpson, Department of Biology, Dalhousie University, 1355 Oxford Street, Halifax, Nova Scotia, Canada B3H 4J1—Telephone number: 902 494 1247; FAX number: 902 494 3736; e-mail: alastair.simpson@dal.ca

croscope equipped with an Axiocam HR digital camera. Lengths and widths of live *H. teleskopos* cells ($n = 17$) were determined from digital micrographs using the camera software (Axiovision 4.6).

Electron microscopy. For freeze substitution, approximately 1.5 ml of cell culture was pelleted at 1,000 *g* for 30 min in a microcentrifuge tube. The supernatant was aspirated and material from the pellet loaded into hexadecene-coated 200 μm-deep gold-plated planchettes for high-pressure freezing using liquid nitrogen. The frozen specimens were transferred, under liquid nitrogen, to sample tubes containing an anhydrous solution of 2.0% (w/v) OsO_4 and 0.1% (v/v) glutaraldehyde in HPLC-grade acetone. The temperature was raised from $-160\,^{\circ}C$ at a rate of $1\,^{\circ}C$/h, holding the temperature steady for ~ 24 h at $-90\,^{\circ}C$ and for ~ 12 h at $-60\,^{\circ}C$. During the $-60\,^{\circ}C$ period, the specimens were removed from the fixation cocktail and placed in pure acetone. Subsequently, the temperature was raised by $2\,^{\circ}C$/h, with a 24-h holding period at $-30\,^{\circ}C$, until the specimens were at $-20\,^{\circ}C$. They were then transferred to $-20\,^{\circ}C$ for ~ 24 h, and then to $4\,^{\circ}C$ for ~ 12 h, before being allowed to warm to room temperature. Specimens were suspended in pure acetone and agitated to remove them from the planchettes; all subsequent handling was done using 1,000 μl micropipettes with cut-off tips. Specimens were transferred through a series of Spurr's resin mixtures (one-third resin, two-thirds resin, and three changes of full resin), before final embedding.

For conventional chemical fixation, cells were centrifuged at 8,000 *g* for 3 min and fixed for 30 min at room temperature in a cocktail containing 1% (v/v) glutaraldehyde, 5% (w/v) sucrose, and 0.1 M cacodylate buffer (pH 7.4). After rinsing the cells 3 times in 0.1 M cacodylate buffer with 5% (w/v) sucrose, cells were post-fixed for 1 h in 0.8% (w/v) OsO_4 and 5% (w/v) sucrose in 0.1 M cacodylate. After being rinsed free of post-fixative, cells were concentrated by centrifugation and trapped in 1.5% (w/v) agarose. Agarose blocks were dehydrated by applying a graded series of ethanols, and then embedded in Spurr's resin.

Serial sections (~ 70 nm) were cut with a diamond knife on a Leica UC6 ultramicrotome (Leica, Knowlhill, Wetzlar, Germany) and were subsequently stained with saturated uranyl acetate in 50% ethanol and with lead citrate. Sections were observed using a Tecnai 12 transmission electron microscope (FEI, Hillsboro, OR, Philips) fitted with a goniometer stage.

SSU rRNA gene sequencing. DNA was isolated using a hexadecyltrimethyl ammonium bromide (CTAB) protocol (Clark 1992). The SSU rRNA gene was amplified using universal eukaryotic primers (Medlin et al. 1988). A fragment of expected size was then purified from the gel and subcloned into pCR4 TOPO vector (Invitrogen, Carlsbad, CA). Four clones were partially sequenced and identity of the sequences was confirmed using BLAST (Altschul et al. 1990). Subsequently, two identical clones were fully bidirectionally sequenced by primer walking. This sequence has been deposited in GenBank as Accession number FJ628363.

Phylogenetic analyses. The master alignment used for this study was constructed using CLUSTALX 1.83 (Thompson et al. 1997). Some sequences were realigned to the main alignment using the program MAFFT (Katoh et al. 2005) with the EINSII algorithm. The alignment was then edited manually in BioEdit 7.0.5.3 (Hall 1999). Ambiguously aligned regions were excluded from analysis; the final trimmed dataset was 827-bp long. The alignment is available upon request.

The main dataset included a wide taxon sampling of diplomonads, representatives of the retortamonad genera *Retortamonas* and *Chilomastix*, plus *C. membranifera*, *D. brevis*, and some uncultured eukaryote sequences similar to Fornicata, including CPS-GM-5 and its relatives (see Takishita et al. 2007). A variety of other eukaryotes was used as an outgroup, including representatives of all other major groups of excavates. We also analysed a second dataset, identical to the first except that the genus *Chilomastix* was excluded. The reason for this was the placement of *Chilomastix* in SSU rRNA gene trees: *Chilomastix* SSU rRNA gene sequences do not form a clade with those from *Retortamonas*, the other member of Retortamonadida, but instead fall at the base of the diplomonad+retortamonad clade (Cepicka et al. 2008). While this pattern could represent the true phylogeny it is also consistent with the *Chilomastix* lineage being more rapidly evolving than *Retortamonas*, and erroneously placed towards the base of the tree as a long-branch attraction artifact. The exact placement of *Chilomastix* within the basal part of the tree is also relatively unstable (Cepicka et al. 2008), which is consistent with this possibility.

Phylogenetic trees were reconstructed using maximum likelihood (ML) and Bayesian methods. For both datasets, the model of sequence evolution (GTR+Γ+I) was selected using the Akaike information criterion, as implemented in the program Modeltest (Posada and Crandall 1998). The ML trees were estimated using PAUP* 4b10 with 10 random taxon additions followed by tree-bisection-reconnection (Swofford 2003), and subsequently bootstrapped with 500 replicates using the program IQPNNI 3.2 (Vinh and von Haeseler 2004). The Bayesian analysis was carried out in MrBayes 3.2 (Huelsenbeck 2000) with two independent runs, each with four independent chains running for 1.4×10^7 generations (a burn-in of 2.5×10^5 generations was used), with default heating parameter (0.2) and sampling frequency (0.01).

RESULTS

Light microscopy. Cells are biflagellated and broadly oval shaped with a longitudinal groove (Fig. 1–4). The groove is difficult to see while the cell is swimming. Cells are 6.5–10.0 μm long (average ± SD 8.5 ± 0.9 μm, $n = 17$) and 4.5–8.0 μm wide (5.8 ± 0.9 μm). The posterior flagellum is 2.5–3.5 times the length of the cell body. It runs through the groove and then trails freely behind the cell (Fig. 1, 2). The second flagellum is directed leftwards and slightly anteriorly, and is approximately 1–1.5 times the cell length (Fig. 3). In phase contrast microscopy the nucleus can be observed in the anterior end of the cell (Fig. 1). Most cells contain vacuoles with prokaryotic contents (Fig. 1, 4). The groove runs along the whole length of the cell body. In the anterior third of the cell the right wall of the groove is sharply defined, and contains a thick cytoskeletal element (presumably, the right root [RR] and B fibre—see ''ultrastructure'' below) that can be observed readily using phase contrast (Fig. 1, 2). The margin then undergoes a bend, causing the groove gradually to narrow posteriorly, and the cytoskeletal element becomes less conspicuous. At the posterior end of the cell, the groove deflects to the left where it continues into the cell as a narrow, difficult-to-observe cytopharynx (Fig. 1, 2). When moving, the cell swims in more or less straight lines, with a rapid rotation about its longitudinal axis.

Ultrastructure. Terms for ultrastructural components are as used by Simpson and Patterson (1999) and Yubuki et al. (2007), except that we identified the flagella and basal bodies numerically, as per O'Kelly (1993) and Simpson (2003). The general appearance of the cells under light microscopy was also observed by transmission electron microscopy. The nucleus and flagellar apparatus are in the anterior part of the cell, with the flagellar apparatus located subapically (Fig. 5, 8). Posterior to the flagellar apparatus is the ventral groove. The edges of the groove are supported by microtubules originating from basal body 1 (Fig. 6–8). The most sharply defined part of the groove is immediately next to its right margin (Fig. 8). We observed one encysted cell in our chemical fixation (Fig. 9). This was approximately rounded with

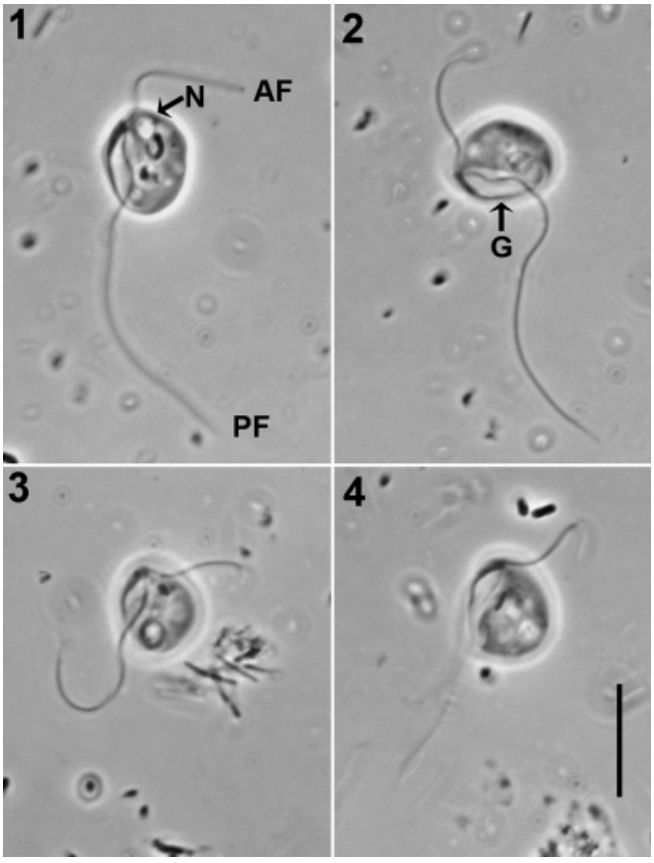

Fig. **1–4.** Phase contrast light micrographs of living cells of *Hicanonectes teleskopos* n. g., n. sp. Note the delicate curving cytopharynx at the posterior end of the groove (**1**), and the flagellar insertion and flagellar lengths (**2, 3**). AF, anterior flagellum; G, groove; N, nucleus; PF, posterior flagellum. Scale bar = 10 μm.

internalized flagellar axonemes and a loose-fitting, relatively thin cyst wall without scales or fibrous materials.

In trophic cells the nucleus is very closely associated with the basal bodies. It is rounded and lacks a central nucleolus; instead, densely staining material is seen concentrated at one end (Fig. 5). No Golgi apparatus was observed. Rounded mitochondrion-like organelles up to 300 nm in diameter were observed throughout the cells (Fig. 5, 8). These lack cristae. However, the organelles were not well preserved, and we could not visualize clearly the bounding membranes (Fig. 10, 11). Some mitochondrion-like organelles appeared to be undergoing division (Fig. 11). Faint parallel striations were sometimes observed in grazing sections of the surface of these organelles (Fig. 12). Food vacuoles with prokaryotic contents were seen in the middle and posterior of the cell (Fig. 5, 8). In some cells we observed small prokaryotes coated with numerous filaments ($\sim$ 300 nm diameter, excepting the filaments), which were free within the cytoplasm and might be endosymbionts (Fig. 13). These prokaryotes were not associated closely with the mitochondrion-like organelles.

Flagellum 1 (i.e. the posterior flagellum) and flagellum 2 (i.e. the anterior flagellum) each have a normal 9+2 axoneme (Fig. 14, 29). The transition between the 9+2 structure and the basal body typically occurs within the cytoplasm, 200–300 nm below the level of insertion (Fig. 17, 19, 20). Flagellum 1 has two vanes, each supported by a fine paraxonemal lamellum (Fig. 14). One vane is very conspicuous and broad (maximum breadth $\sim$ 600 nm), and is located on the ventral side of the axoneme, while the second vane is much smaller and is located on the dorsal side (Fig. 14, 15). The ventral vane originates near the flagellar insertion (Fig. 15). The dorsal vane originates more distally. The outer edge of the ventral vane has a striated appearance in grazing section, with the striations arranged perpendicular to the axoneme (Fig. 16). There are normally four basal bodies in the flagellar apparatus (Fig. 17, 39), each with a normal triplet structure (Fig. 18, 25, 33). Basal bodies 1 and 2 give rise to flagellum 1 and 2, respectively, and are about 330 nm in length (Fig. 17, 19, 20). Basal bodies 3 and 4 are normally non-flagellated, and they are sometimes shorter than the flagellated basal bodies. All basal bodies have a short ($\sim$ 70 nm) cartwheel structure (e.g. Fig. 33). The flagellated basal bodies 1 and 2 are arranged at a slightly obtuse angle (Fig. 19, 39) and are separated by $\sim$ 50 nm at their closest (Fig. 18). Basal body 2 is directed leftwards and somewhat anteriorly. Non-flagellated basal body 3 is situated close and nearly parallel to basal body 2, but is located more ventrally (Fig. 18, 39). Non-flagellated basal body 4 lies to the left of basal body 1 and is directed leftwards (Fig. 17, 39).

There is one microtubular root, the anterior root (AR), associated specifically with basal body 2. The AR originates adjacent to the right/anterior side of basal body 2, in association with fibrous and dense material on its interior side (Fig. 18, 21, 39). Additional fibrous material also connects basal body 2 to basal body 1 (Fig. 21). The AR extends to the left-dorsal side of basal body 2 together with the dense material (Fig. 21, 39). The number of microtubules in the AR gradually increases at a rate of roughly one per transverse section ($\sim$ 70 nm), up to nine microtubules (Fig. 22). There is a dorsal fan of individual microtubules associated with the AR (Fig. 19, 20, 39). These appear to originate alongside and parallel to the AR, and support the cell membrane outside the confines of the groove. Two clusters of individual internal microtubules (IMt), IMt1 and IMt2, originate from different microtubular organizing centres (MTOCs), which are closely associated with the proximal ends of basal bodies 3 and 4, respectively (Fig. 23, 27, 28, 39).

Basal body 1 is linked to two major microtubular roots, the left root (LR) and the right root (RR), as well as a singlet microtubular root, and some non-microtubular fibres (e.g. B, I, A, and C fibres; Fig. 24, 25, 39). The RR originates aligned to the right side of basal body 1 (Fig. 24–26, 39), although its proximal (anterior) end is also closely associated with basal body 2 and the proximal end of the AR (Fig. 19). It expands rapidly to include about 20 microtubules in a single curved row (Fig. 24). Slightly posterior to the opening of the groove, the RR splits into an inner portion of seven microtubules (IRR) and an outer portion of 13 microtubules (ORR, Fig. 29, 30, 39). The ORR curves around to form part of the support for the right wall of the groove, while the IRR remains associated with the floor of the groove (Fig. 29, 31, 39). More distal sections of the right wall of the groove show up to 24 microtubules, representing a combination of ORR-derived microtubules, IMt1, and possibly some dorsal fan microtubules (Fig. 32). The material that we identify as the A fibre is closely associated with the dorsal side of the RR, was seen only at the proximal end of the RR, and is quite indistinct (Fig. 25). The I fibre is closely associated with the ventral side of the RR (Fig. 24–27, 39). It is composed of a double-leaved sheet connected to the ventral face of the RR by a latticework structure, and has a total thickness of $\sim$ 40 nm (Fig. 24). Posterior to the split of the RR, the I fibre continues only with the outer portion of the ORR (Fig. 28–31). The B fibre material has two distinct elements. The first element has a laminate appearance in transverse section. This element originates from the right side of the LR, then arches across the ventral side of basal body 1 to become closely associated with the RR (Fig. 24, 26, 39). The second element appears as a dense amorphous sheet with a relatively lucent field associated with its

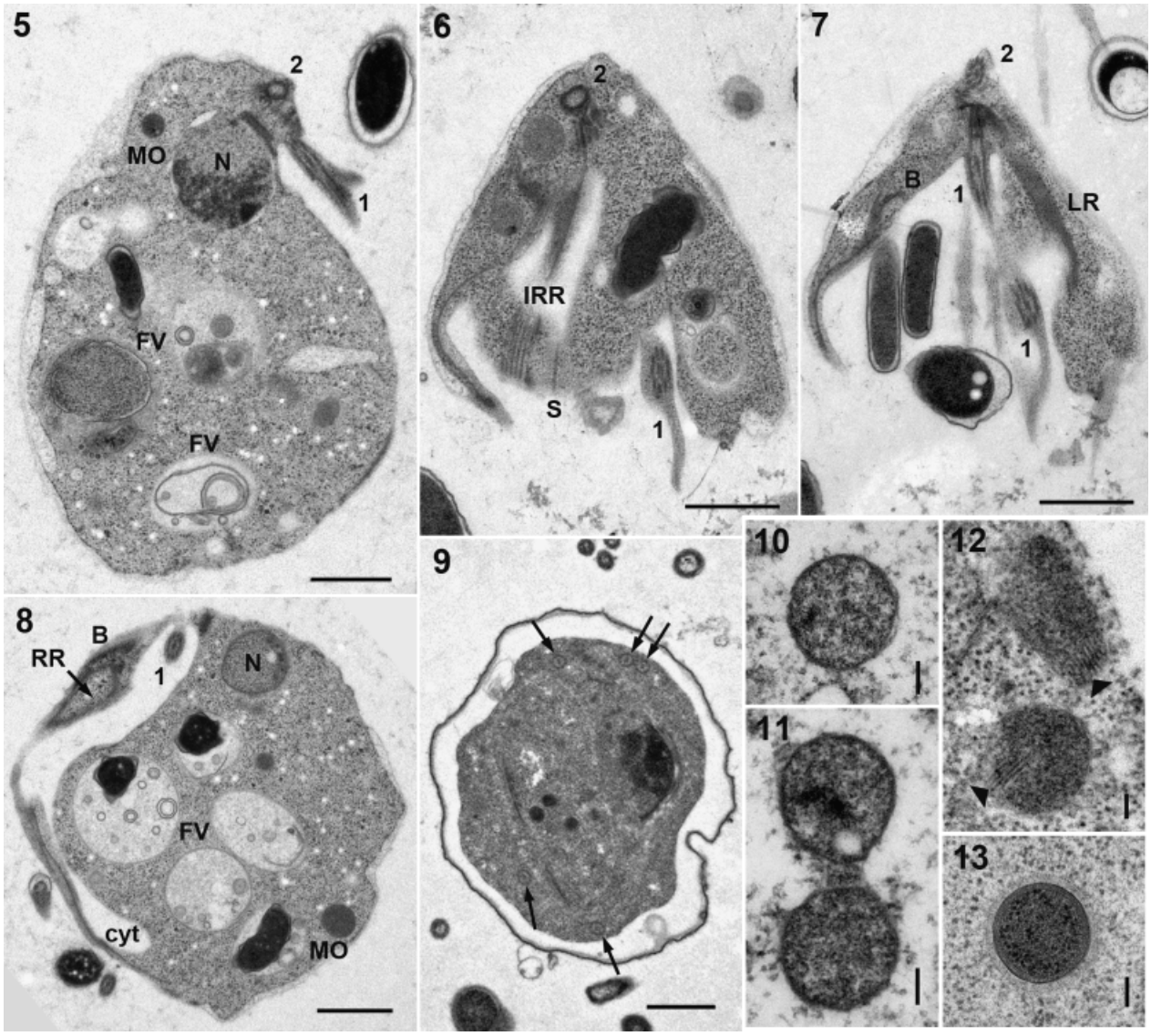

Fig. **5–13.** Transmission electron micrographs of *Hicanonectes teleskopos* n. g., n. sp., ultra-thin sections. **5–8.** Cells in longitudinal sections. 5. Lateral view; 6–8. Ventral view. **9.** Cyst showing flagellar axonemes (arrows) within the cytoplasm (chemical fixation). **10–12.** Mitochondrion-like organelles (10, 11: chemical fixation). Arrowheads in 12 indicate faint parallel striations in the surface of the organelles. **13.** Intracytoplasmic prokaryote surrounded by numerous filaments. 1, flagellum/basal body 1 (= posterior flagellum/basal body); 2, flagellum/basal body 2 (= anterior flagellum/basal body); B, B fibre, cyt: cytopharynx; FV, food vacuole; IRR, inner portion of right root; LR, left root; MO, mitochondrion-like organelle; N, nucleus; RR, right root; S, singlet microtubular root. Scale bars for 5–9 = 1 μm; for 10–13 = 100 nm.

ventral face (Fig. 28–31, 39). This second element projects orthogonally from the ventral face of the laminate element (Fig. 33, 39). The laminate element ends near the opening of the groove, while the dense element runs posteriorly immediately under the cell membrane of the right margin of the groove (Fig. 27–29, 31). Initially the dense element of the B fibre runs parallel to the RR and the I fibre (Fig. 27, 28). The subsequent curvature of the RR means that the RR and the I fibre end up arranged perpendicular to the B fibre (Fig. 31). The singlet microtubular root (S) originates close to basal body 1 and the dorsal side of the RR (Fig. 24, 26, 34, 39). It continues posteriorly, close to but separate from the left side of the RR (Fig. 27–29).

The LR is composed of a single row of 10 microtubules that are closely linked to the non-microtubular C fibre (Fig. 27–29, 39). The C fibre adheres to the dorsal side of the LR (Fig. 24, 25, 27, 39). It appears as one dense and one fine sheet in transverse section, and is about 40 nm thick (Fig. 27). The C fibre ends at the level of the opening of the groove. Slightly posterior to this, an additional microtubule originates close to the dorsal side of the LR, and runs parallel to the main LR microtubules (Fig. 28).

As the groove broadens, its right margin is supported primarily by the B fibre and the ORR (Fig. 7, 8, 29, 39). The outer side of this groove wall is also supported by IMt1 microtubules (Fig. 37). The left wall of the groove is supported by the LR (Fig. 7, 39). The right half of the floor of the groove is supported by the singlet root, the IRR, and a few microtubules that originate from the ORR (Fig. 6, 29). The left half of the groove is supported by sparse microtubules derived from the LR and IMt2. Farther down the groove, the I fibre and B fibre are reduced and then lost (Fig. 32). Halfway down the groove, there is a bend in the right wall (Fig. 6–8).

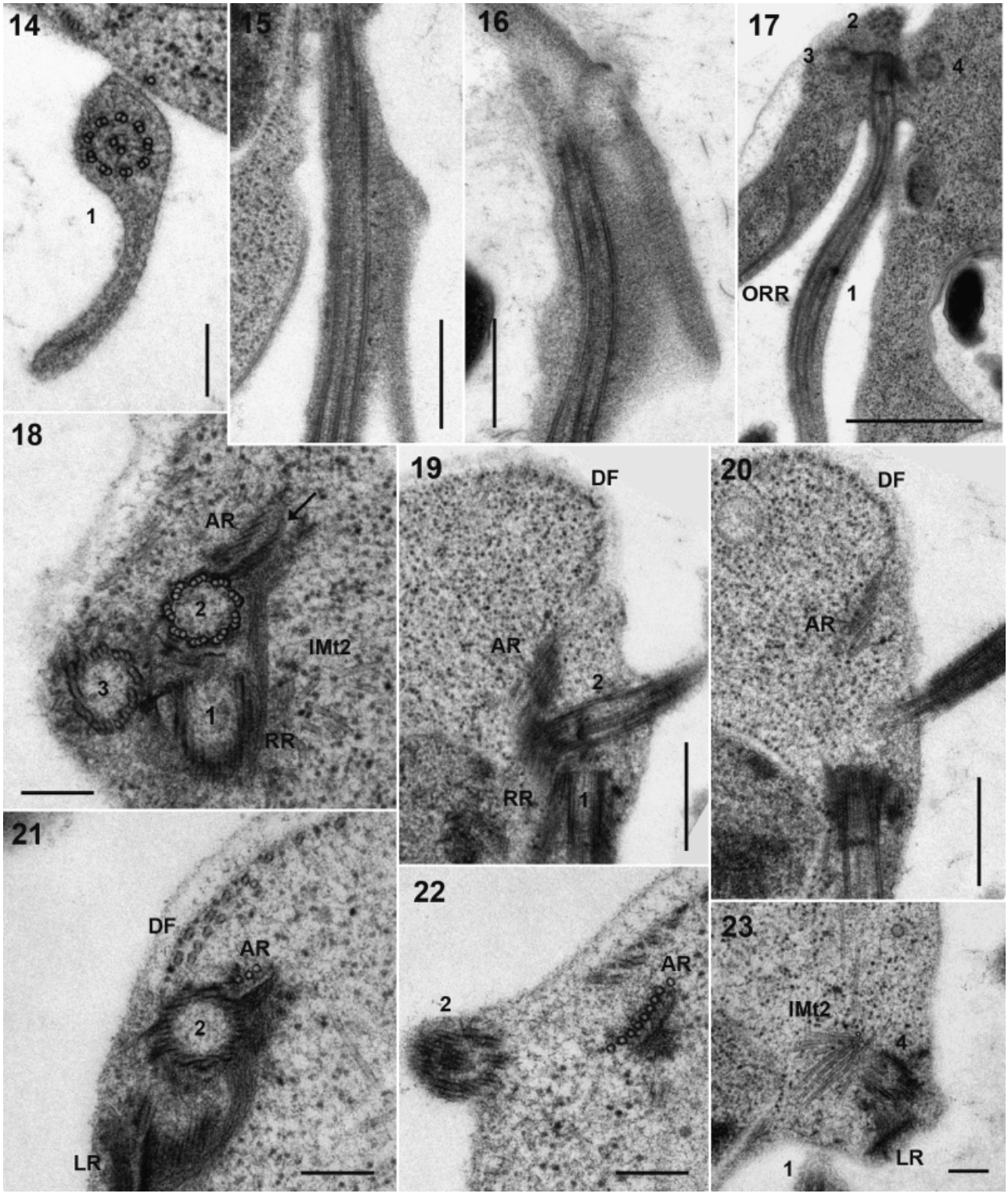

Fig. **14–23.** Transmission electron micrographs of *Hicanonectes teleskopos* n. g., n. sp., ultra-thin sections. **14.** Posterior flagellum in transverse section showing normal 9+2 axoneme structure and two flagellar vanes (ventral much larger than dorsal). **15, 16.** Posterior flagellum in longitudinal section, showing the origin of the ventral vane shortly after emergence (15), and the striated appearance of the outer portion of the ventral vane (16). **17.** Longitudinal section through the anterior portion of the cell, showing four basal bodies (i.e. 1–4). **18.** Section showing triplet structure of basal bodies 2 and 3. Note the anterior root (AR) and electron-dense material originating adjacent to basal body 2. **19, 20.** Near-consecutive sections showing the AR associated with the dorsal fan. Note the anterior end of the right root (RR) located close to basal body 2 and the AR. **21, 22.** Near-consecutive transverse sections of AR, showing origin of the root and number of microtubules, and electron-dense material around the basal bodies. **23.** IMt2 originating from an MTOC near basal body 4. 1, flagellum/basal body 1 (= posterior flagellum/basal body); 2, flagellum/basal body 2 (= anterior flagellum/basal body); 3, non-flagellated basal body 3; 4, non-flagellated basal body 4; DF, dorsal fan; IMt 2, radiation of internal microtubules; LR, left root; ORR, outer portion of right root; MTOC, microtubular organising centre. Scale bars for 14, 18, 21, 22, and 23 = 200 nm; for 15, 16, 19, and for 20 = 500 nm; for 17 = 1 μm.

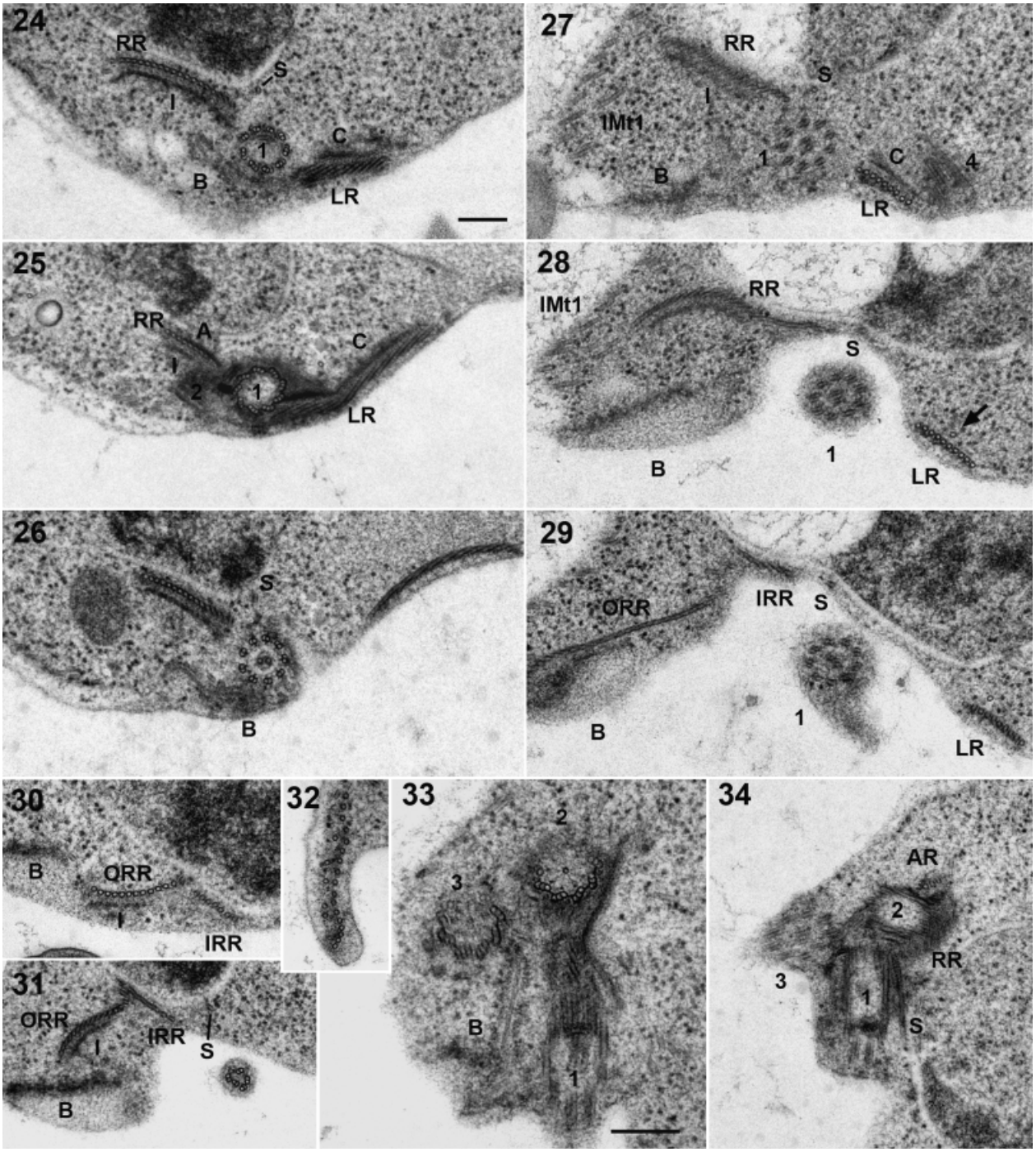

Fig. **24–34.** Transmission electron micrographs of *Hicanonectes teleskopos* n. g., n. sp., ultra-thin sections. **24.** Transverse section of basal body 1 showing RR and LR, singlet microtubule, and associated non-microtubular fibres. Note the origin of the lamellate element of the B fibre against the LR. **25, 26.** Non-consecutive serial sections showing basal body 1 and associated fibres. Note the A fibre (in 25), indistinct by the level of the transition zone (26). **27–29.** Non-consecutive serial sections showing the LR in transverse section, as well as the outer portion of the RR and anterior end of the groove. The RR separates into outer and inner portions near the opening of the groove. Arrow in 28 indicates an additional single microtubule parallel to dorsal side of the left root, posterior to the termination of the C fibre. **30.** Transverse section of the IRR and ORR, showing the maximal number of microtubules. **31.** Section showing the angle between the IRR and ORR, and the normal position of the amorphous element of the B fibre. **32.** Transverse section showing right side of the groove, after the termination of the B fibre. The groove wall is supported by microtubules originating from the ORR, as well as IMt1. **33.** Section showing the relationship between the two distinct elements of the B fibre (i.e. one with laminate appearance and the other including electron-dense sheet and amorphous material). Note also the cartwheel structures in basal bodies 2 and 3. **34.** Section showing the origin of the singlet microtubular root. 1, flagellum/basal body 1 (= posterior flagellum/basal body); 2, basal body 2 (= anterior basal body); 3, non-flagellated basal body 3; 4, non-flagellated basal body 4; A, A fibre; AR, anterior root; B, B fibre; C, C fibre; I, I fibre; IMt1, radiation of internal microtubules; IRR, inner portion of right root; LR, left root; ORR, outer portion of right root; RR, right root; S, singlet microtubular root. Scale bars (in 24) = 200 nm for all figures except 33, for in 33 = 200 nm.

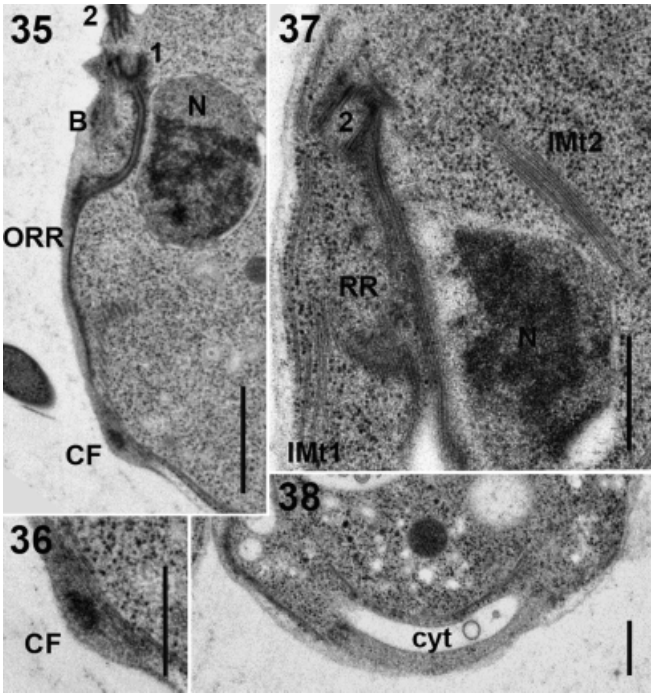

Fig. **35–38.** Transmission electron micrographs of *Hicanonectes teleskopos* n. g., n. sp., ultra-thin sections. **35.** Longitudinal section showing the right wall of the groove. Note the position of the possible composite fibre. **36.** Higher magnification view of the possible composite fibre. **37.** Section showing elements of IMt1 and IMt2. **38.** Posterior end of the cell, showing the cytopharynx. 1, basal body 1 (= posterior basal body); 2, flagellum/basal body 2 (= anterior flagellum/basal body); B, B fibre; CF, composite fibre; cyt, cytopharynx; IMt1 and IMt2, radiations of internal microtubules; N, nucleus; ORR, outer portion of right root; RR, right root. Scale bars for 35 = 1 μm; for 36–38 = 500 nm.

Posterior to this point, the right wall includes a small non-microtubular fibre, which we interpret to be the composite fibre (Fig. 35, 36). The cytopharynx is located in the posterior portion of the cell, and is supported by several microtubules originating ultimately from the RR (Fig. 8, 38).

Molecular phylogeny. In our analyses we included 36 sequences from Fornicata (including seven environmental sequences) and an outgroup of 32 other eukaryotes (Fig. 40a). The overall topology of Fornicata is mostly consistent with recently published results (e.g. Cepicka et al. 2008; Keeling and Brugerolle 2006; Kolisko et al. 2005, 2008; Yubuki et al. 2007). The monophyly of Fornicata, including our new isolate, was highly supported, with 96% bootstrap support (BS) and posterior probability (PP) of 1. Within Fornicata a major clade was recovered that included all diplomonads and the retortamonad *Retortamonas*, but not the retortamonad *Chilomastix*. The monophyly of diplomonads+*Retortamonas* was highly supported (99% BS; 1 PP), as was the monophyly of hexamitine diplomonads, including enteromonads (100% BS; 1 PP). The genus *Retortamonas* branches weakly with the giardiine diplomonads *Giardia* and *Octomitus* (46% BS; 0.77 PP).

The other fornicates, including our new isolate, formed a series of branches attached to the base of the diplomonads+*Retortamonas* clade. In order, these were (i) *Chilomastix* spp., (ii) *D. brevis*, (iii) a clade comprising *C. membranifera*, our new isolate, and uncultured eukaryote D4P08A09, and (iv) a tight clade consisting of several sequences from uncultured eukaryotes, including CPS-GM5, whose close relative was identified as a *Carpediemonas*/*Dysnectes*-like excavate using light microscopy (Takishita et al. 2007). The branching pattern among these clades, however, received low or very low BS.

Our new isolate formed a highly supported clade with uncultured eukaryote sequence D4P08A09 (100% BP: 1 PP). These two sequences in turn formed a clade with *C. membranifera* that received moderate BS (70%), and PP 1. It is noteworthy that sequence D4P08A09 was obtained from anoxic intertidal marine sediments, a similar environment to that from which both our new isolate and *C. membranifera* were originally isolated.

We repeated the analysis without the sequences from the retortamonad *Chilomastix* (Fig. 40b). A similar ML topology was recovered, and most important nodes received similar statistical support, with two exceptions. Firstly, the BS for the monophyly of *Carpediemonas*, our new isolate, and uncultured eukaryote D4P08A09 increased to 86% (PP remained at 1). Secondly, support for the placement of *D. brevis* as the sister group to diplomonads+retortamonads increased to 80% BS (up from 46%), and PP 1 (up from 0.94).

DISCUSSION

The affinities and assignment of *Hicanonectes*. Simpson (2003) recognized an assemblage of flagellates called ''typical excavates'' that share eight distinctive morphological characters (see also O'Kelly 1993, 1997; O'Kelly and Nerad 1999; Simpson and Patterson 1999; Yubuki et al. 2007). These features are (1) a ventral groove used for suspension feeding, (2) flagellar vanes, (3) a splitting of the RR, (4) an I fibre, (5) a B fibre, (6) a singlet microtubular root associated with basal body 1, (7) a C fibre, and (8) a composite fibre. Our new isolate displays at least seven of these characters (Table 1). The sole uncertainty concerns the composite fibre: we identified a delicate non-microtubular element in the same position as the composite fibre of typical excavates, but did not determine its substructure. There are also no data as to whether the typical excavate *Malawimonas* has a composite fibre (O'Kelly and Nerad 1999; Simpson 2003). Other aspects of the ultrastructure of our new isolate are similar to previously studied typical excavates: for example, the arrangement of the left, right, and singlet roots in their support of the feeding groove, and the presence of a detectable A fibre (Simpson 2003; Simpson and Patterson 1999). Based on morphology we consider our new isolate to be a typical excavate, along with jakobids, retortamonads, *Trimastix*, *Malawimonas*, *Carpediemonas*, and *Dysnectes* (Simpson 2003; Yubuki et al. 2007). However, assignation of an organism as a typical excavate does not resolve its phylogenetic position, because molecular phylogenies demonstrate clearly that typical excavates are not a monophyletic group (Dacks et al. 2001; Rodriguez-Ezpeleta et al. 2007; Simpson et al. 2002b, 2006).

Our SSU rRNA gene phylogenies place our new isolate in the clade Fornicata, which includes the typical excavates Retortamonadida, *Carpediemonas*, and *Dysnectes*, as well as the non-typical excavate group Diplomonadida (Cepicka et al. 2008; Simpson et al. 2002b, 2006; Yubuki et al. 2007). Statistical support for this position is strong irrespective of phylogenetic method, and withstands minor changes in taxon sampling. Furthermore the B fibre complex in our new isolate originates against the LR and then arches across the ventral face of basal body 1 to associate with the RR. This arrangement is characteristic of *Carpediemonas*, *Dysnectes*, and retortamonads, and is the proposed synapomorphy that defines the taxon Fornicata (Simpson 2003; Simpson and Patterson 1999; Yubuki et al. 2007).

Some other conspicuous ultrastructural features are consistent with, although not diagnostic of, placement with Fornicata. Our new isolate has two opposed vanes, dorsal and ventral, on its

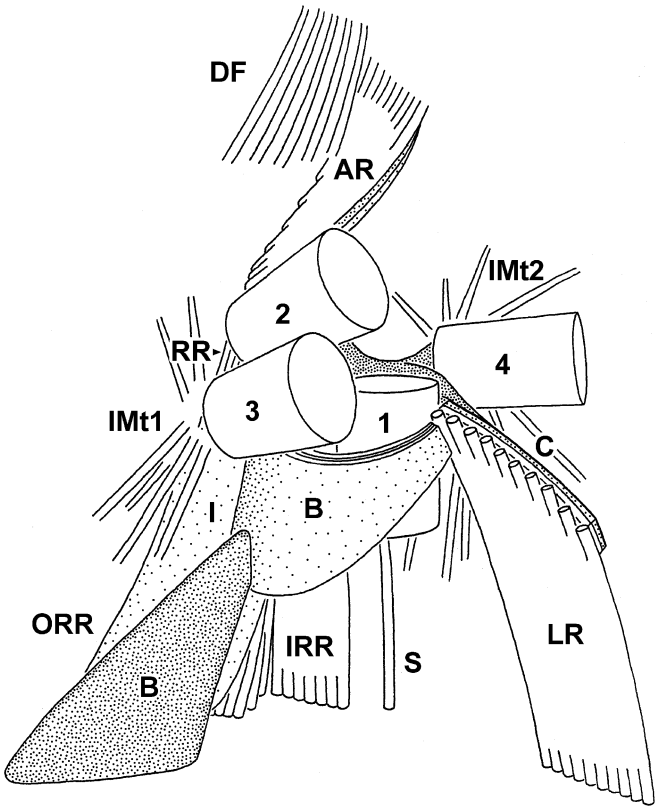

Fig. **39.** Diagrammatic representation of the proximal flagellar apparatus of *Hicanonectes teleskopos* n. g., n. sp., viewed from the ventral side. Basal bodies are depicted as large cylinders and the flagella themselves are not shown. The lucent field associated with the ventral side of the amorphous element of the B fibre has been omitted. All major microtubular roots continue beyond the confines of the diagram. 1, basal body 1 (= posterior basal body); 2, basal body 2 (= anterior basal body); 3, non-flagellated basal body 3; 4, non-flagellated basal body 4; AR, anterior root; B, B fibre; C, C fibre; DF, dorsal fan; I, I fibre; IMt1 and IMt 2, radiations of internal microtubules; IRR, inner portion of right root; LR, left root; ORR, outer portion of right root; RR, right root; S, singlet microtubular root.

posterior flagellum, although the dorsal vane is poorly developed. This is similar to all typical excavate groups except jakobids and *Malawimonas jakobiformis*, which each have only one of the vanes (Lara, Chatzinotas, and Simpson 2006; O'Kelly 1997; O'Kelly and Nerad 1999; Simpson and Patterson 2001). In place of classical-looking mitochondria, our new isolate has rounded organelles that lack cristae. This is similar to other Fornicata, but also to Preaxostyla and Parabasala, none of which have classical crista-bearing mitochondrial organelles (Brugerolle and Patterson 1997; Carpenter, Waller, and Keeling 2008; Hampl and Simpson 2008; O'Kelly, Farmer, and Nerad 1999; Simpson and Patterson 1999; Yubuki et al. 2007). In summary, both molecular phylogenies and easy-to-interpret morphological characters indicate that our new isolate belongs to the taxon Fornicata.

Of the previously described groups within Fornicata, our new isolate is most similar at the ultrastructural level to *Carpediemonas* and *Dysnectes*. It shares with *C. membranifera* 11 of the 13 ultrastructural features highlighted in Table 1 (see also Fig. 41). Like *C. membranifera* our new isolate has an I fibre that includes a double-leaved sheet, while the A fibre is indistinct. However, there are several differences. Our new isolate has four basal bodies, two flagellar vanes, and conspicuous radiations of IMt, whereas *C. membranifera* has three basal bodies, three vanes, and few IMt (Simpson and Patterson 1999). The AR of *C. membranifera* is more delicate, and has a different orientation and relationship to the dorsal fan. The RR and LR of *C. membranifera* consist of 16 and six microtubules, respectively, while those of our new isolate comprise 20 and 10 microtubules, respectively. In *C. membranifera*, most of the width of the groove is supported by microtubules derived ultimately from the RR, whereas microtubules from the RR support only about half the width of the groove in our new isolate. *Carpediemonas membranifera* does not have a distinct cytopharnyx at the posterior end of the groove, while our new isolate has no observable dictyosome.

Our new isolate and *D. brevis* share 10 of the 13 ultrastructural features of excavates (Table 1, see also Fig. 41). The number of microtubules in the RR is similar (18 vs. 20), as is the proportion of the groove supported by microtubules derived from the RR (about half). Both species have two flagellar vanes, while dictyosomes have not been found in either. As with both our new isolate and *C. membranifera*, the A fibre of *D. brevis* is indistinct at best (Yubuki et al. 2007 report it as absent). However, *D. brevis* has two basal bodies in interphase, not four as in our new isolate. The LR of *D. brevis* is more strongly developed, with more microtubules (17 vs. 10), and a thicker C fibre, as well as an extension of the B fibre down its ventral face. *Dysnectes brevis* lacks a distinct cytopharynx. Furthermore, *D. brevis* has a much less substantial AR, and apparently no dorsal fan at all (Yubuki et al. 2007).

As indicated by our SSU rRNA gene phylogenies, our new isolate is markedly dissimilar at the sequence level to other described fornicate taxa. Our ML and Bayesian trees place it as the sister group of *C. membranifera*, along with a related though distinct environmental sequence. Bootstrap support is moderate or strong, depending on taxon sampling. Tentatively, we consider it most likely that *C. membranifera* is the closest formally described relative of our new isolate. Nonetheless, in light of the considerable morphological differences and SSU rRNA gene sequence dissimilarity between our new isolate and *C. membranifera*, we propose that it represents a distinct genus from *Carpediemonas* (and *Dysnectes*). Because we are not aware of any previously described organism with which our isolate can be identified, we here introduce the new genus and new species *H. teleskopos* n. g., n. sp. Formal diagnoses are given at the end of the discussion.

The anterior root and dorsal fan. The AR of *H. teleskopos* n. g., n. sp. is well developed, with nine microtubules attached to a supporting non-microtubular fibre. This root travels anteriorly, and the dorsal fan appears to originate alongside it, in parallel. This organization differs markedly from that in most typical excavates including other fornicates. In *Carpediemonas* and *Dysnectes*, as well as in *Malawimonas* and *Trimastix pyriformis*, the AR curves to run posteriorly down the left side of the cell, contains only one to four microtubules, and is, at most, lightly reinforced with non-microtubular material (Brugerolle and Patterson 1997; O'Kelly and Nerad 1999; O'Kelly et al. 1999; Simpson and Patterson 1999; Yubuki et al. 2007). The dorsal fan, where present, originates along the length of the AR in these taxa. In retortamonads and jakobids, there is no true AR. The dorsal fan originates in close association with basal body 2 in jakobids (Lara et al. 2006; O'Kelly 1997; Patterson 1990), and with the sheet-like non-microtubular ''lapel'' in retortamonads (Bernard, Simpson, and Patterson 1997; Brugerolle 1973). There are some parallels between *H. teleskopos* and *Trimastix marina*. In *T. marina* the AR is also large (15–16 microtubules), is directed anteriorly, and is associated with non-microtubular material (Simpson, Bernard, and Patterson 2000). However, the non-microtubular material is associated with the exterior-most face of the AR, rather than the interior-most face as in *H. teleskopos*, and the dorsal fan is most closely associated with the face of the AR, and not the edge of the root as in *H. teleskopos*. Most likely the AR of ancestral typical

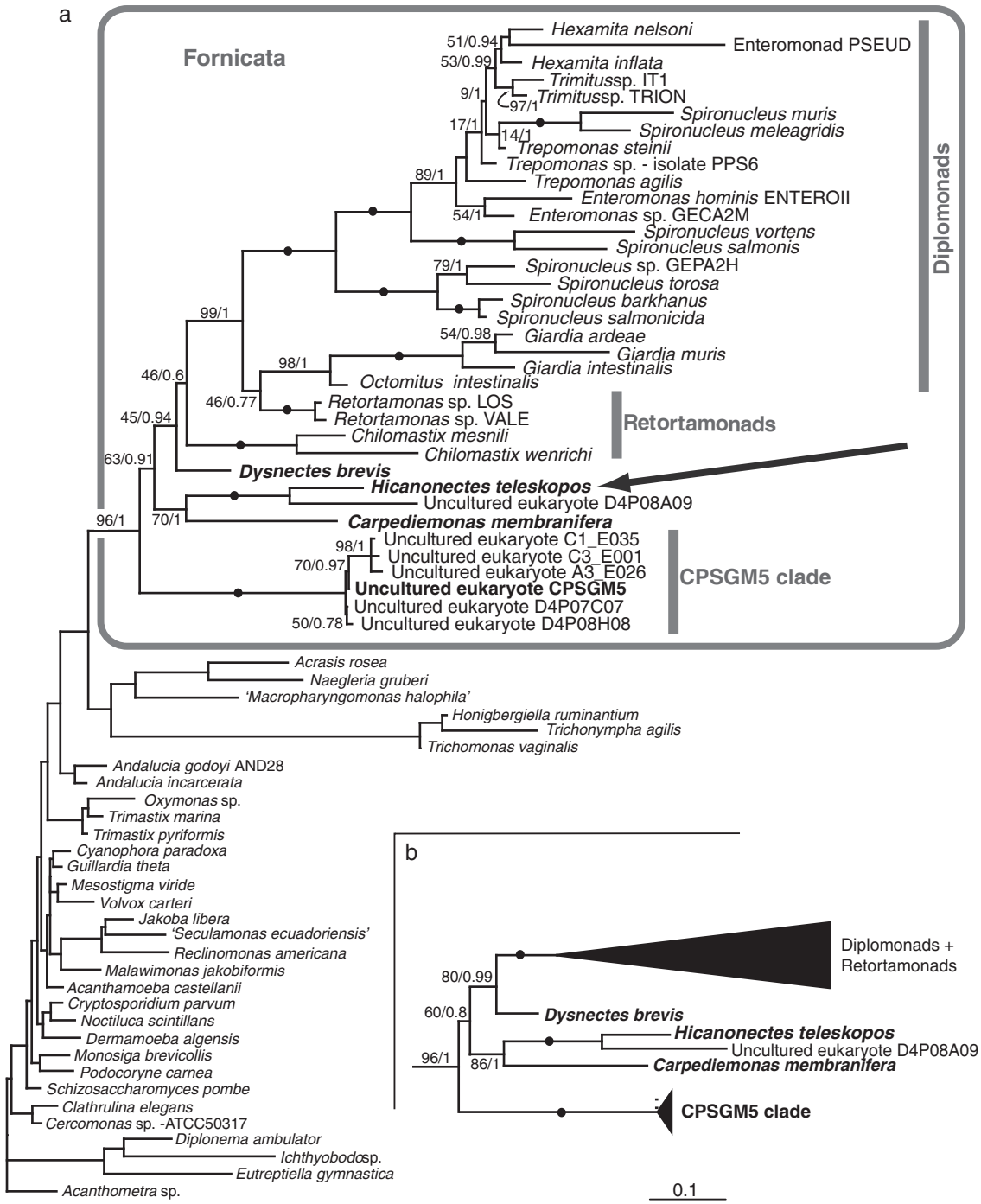

Fig. **40.** Molecular phylogeny of Fornicata showing the position of *Hicanonectes teleskopos* n. g., n. sp. **a.** Maximum likelihood (ML) tree based on the full dataset of SSU rRNA gene sequences (GTR+Γ+I model). **b.** Maximum likelihood topology within Fornicata when *Chilomastix* was excluded from the analysis. Numbers along branches show ML IQPNNI bootstrap percentages and Bayesian posterior probabilities. Support values for nodes outside Fornicata are not shown. Statistical support is not shown for nodes within diplomonads or the CPSGM5 clade when bootstrap support is $<50\%$ and posterior probability is <0.8. Black circles indicate bootstrap support of 100% and posterior probability of 1.

excavates was small and directed leftwards and posteriorly, with *H. teleskopos* and *T. marina* representing two independent lineages in which the AR convergently expanded in size, become more anteriorly directed, and associated differently with the dorsal fan.

The B fibre. In *H. teleskopos* n. g., n. sp., there are two distinct components to the B fibre complex: a laminate sheet-like element, which might be considered the B fibre sensu stricto, and a second, more diffuse element consisting of a dense non-laminate sheet and a relatively lucent zone. It is this second element that extends further posteriorly and associates most closely with the right margin of the groove. The B fibre of *D. brevis* appears also to comprise two distinct elements (fig. 16, 17, 24, and 25 in Yubuki et al. 2007). Although not explicitly identified previously, the second

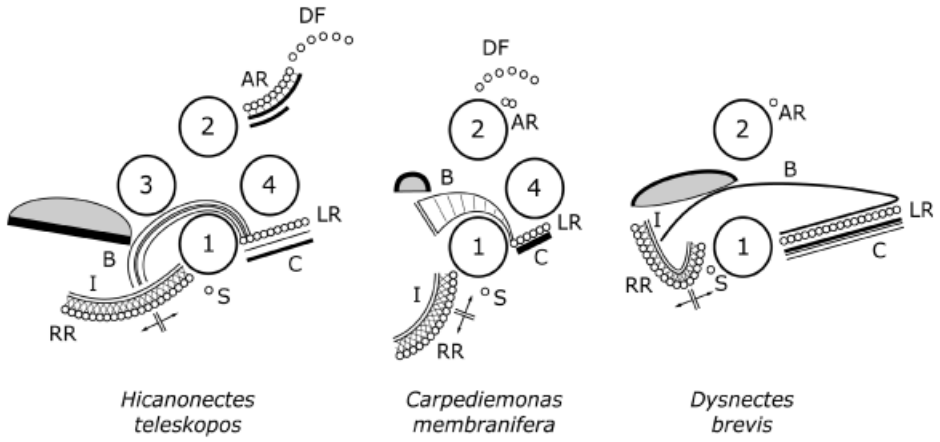

Fig. **41.** Diagrams of the flagellar apparatus of basal fornicates, using the system of Sleigh (1988), as per Simpson (2003). Each basal body is represented in tip-to-base orientation, and its associated microtubules and non-microtubular structures are aligned with it. Not all non-microtubular structures are shown (e.g. possible A fibres are omitted). Note that not all structures shown are present at the same level of sectioning; microtubular roots are shown at their fullest extent, although they frequently gain or lose microtubules along their length. Note also that non-microtubular elements, especially the B fibre, may not be present in the shape indicated in all planes of section; in *Dysnectes* it runs along the outermost six or so microtubules of LR as that root increases from 1 to 17, and is not present at all along more-inward microtubules. *Dysnectes* is depicted from information in Yubuki et al. 2007; *Carpediemonas* after Simpson 2003, with reference to original micrographs (Simpson and Patterson 1999). 1, basal body 1 (= posterior basal body); 2, basal body 2 (= anterior basal body); 3, non-flagellated basal body 3; 4, non-flagellated basal body 4; B, B fibre; C, C fibre; DF, dorsal fan; I, I fibre; LR, left root; RR, right root; S, singlet microtubular root.

element may also be present in *C. membranifera* (fig. 3f, g and 4b–f in Simpson and Patterson 1999). The precise appearance of this element differs in all three species, although some of this variation might be due to different fixation protocols. The presumed homologue of the B fibre in retortamonads is the structure originally referred to as the arched fibre (Simpson 2003; Simpson and Patterson 1999). This fibre has a second discrete element of amorphous material that is associated with its ventral face, and which lies within the right margin of the anterior part of the groove (Bernard et al. 1997; Brugerolle 1977). This extra material might be homologous to the second element of the B fibre complex of *Hicanonectes*, *Carpediemonas*, and *Dysnectes*. We have not identified a positionally equivalent element in other typical excavates. There is an amorphous element associated with the B fibre in the jakobid *Andalucia incarcerata*, but this is sandwiched between the I fibre and B fibre, rather than being at the right margin of the groove wall (Simpson and Patterson 2001), and is unlikely to be homologous.

Mitochondrion-like organelles. The mitochondrion-like organelles of *H. teleskopos* n. g., n. sp., are rounded and of moderate size, $\sim$ 300 nm across, and they are common within the cell. This is similar to the mitochondrion-like organelles of *D. brevis* (Yubuki et al. 2007). In *C. membranifera* the mitochondrion-like organelles are elongate rather than rounded, and may be connected as a network, but are otherwise similar (Simpson and Patterson 1999). The organelles in all three taxa are much larger than the mitosomes of the diplomonad *G. intestinalis*, which are apparently not involved in ATP generation (Tovar et al. 2003). In biovolume, the organelles of *H. teleskopos*, *D. brevis*, and *C. membranifera* are more similar to the hydrogenosomes of

Table **1.** Summary of the structural features of *Hicanonectes teleskopos* n. g., n. sp. and other excavates.

Taxon	Ventral groove	Flagellar vanes (#)	Split RR	I fibre	B fibre (origin)	SR	C fibre (# sheets)	CF	A fibre	Number of basal bodies	AR	Dorsal fan	Mitochondrial organelle
Hicanonectes	+	+ (2)	+	+	+ (LR)	+	+ (2)	+	+	4	+	+	NC
Carpediemonas	+	+ (3)	+	+	+ (LR)	+	+ (2)	+	+	3	+	+	NC
Dysnectes	+	+ (2)	+	+	+ (LR)	+	+ (3)	+	?[a]	2	+	–	NC
Retortamonads	+	+ (2/3)	+	+	+ (LR)	+	+ (2)	+	+	4	–	+	NC
Trimastix	+	+ (2)	+	+	+ (RR)	+	+ (2)	+	+	4	+	+	NC
Malawimonas	+	+ (1)	+	+	+ (BB)	+	+ (4)	+	+	2	+	+	C
Jakobids	+	+ (1)	+	+	+ (BB)	+	+ (1)	+	+	2	–	+	C (1 NC)
Diplomonads	+	–[b]	+	+	–	?	–	–	?	4	+	–	NC
Parabasalids	–	–	–	–	–	–	?	–	?	Varies	–	+	NC
Oxymonads[c]	–	–	–	+	+ (RR)	+	+ (2)	–	?	4	+	+	NC
Euglenozoa	–	–	–	–	–	–	–	–	?	2	+	+	C (mostly)
Heterolobosea	±	–[b]	+	+	–	–	–	–	?	2/4	?	+	C (mostly)

''Typical excavates'' are shaded grey.

[a]Recorded as absent by Yubuki et al. (2007), but see Figure 16 in Yubuki et al. (2007) for a possible delicate A fibre.

[b]Probably non-homologous flagellar vanes in one isolated subgroup – see O'Kelly (1997), Simpson (2003).

[c]Based on the underived oxymonad *Monocercomonoides*—see Simpson et al. (2002b).

+, present; –, absent; ?, uncertain; AR, anterior root; BB, basal body; C, cristae in mitochondrion-like organelles; CF, composite fibre; LR, left root; NC, no cristae in mitochondrion-like organelles; RR, right root; SR, singlet root.

parabasalids, but are somewhat smaller than the typical ~ 500 nm diameter (e.g. see Benchimol 2008). They also resemble the mitochondrion-related organelles of the preaxostylan excavate *T. pyriformis* (Brugerolle and Patterson 1997; O'Kelly et al. 1999), which might also perform hydrogenosomal ATP generation (based on the presence of transcripts for PFO (pyruvate: ferredoxin oxidoreductase and [FeFe]-hydrogenase, Hampl et al. 2008). Overall, this study confirms that Fornicata is a lineage in which classical mitochondria are universally absent, yet contains a series of organisms with mitochondrion-like organelles that differ in appearance from the mitosomes of *Giardia*. Further studies of these organisms may help clarify how the *Giardia* mitosome evolved from presumably less-reduced mitochondrion-like organelles.

The relationships among Fornicata. A well-sampled and well-resolved phylogenetic tree of Fornicata is required for understanding important aspects of the evolution of this group (e.g. possible transitions between different types of mitochondrion-like organelles), and developing a rational higher taxonomy of its more recently discovered major lineages. The deep portions of the Fornicata tree are presently not well-resolved using SSU rRNA gene data. We recovered a *Hicanonectes*+*Carpediemonas* clade with reasonable statistical support, but found mostly poor support for the relationships among (i) the *Hicanonectes*+*Carpediemonas* clade, (ii) *Dysnectes*, (iii) the clade including CPSGM-5, (iv) a diplomonad+*Retortamonas* clade, and (v) *Chilomastix*, where included. We did recover a *Dysnectes*+diplomonad+retortamonad clade with high PP, and with reasonably strong BS when *Chilomastix* was excluded. We suggest that an unstable position of *Chilomastix* was masking otherwise moderate-to-strong support for the *Dysnectes*+diplomonad+retortamonad clade. However, our tree topology conflicts with the analysis of Yubuki et al. (2007) where *Dysnectes* was recovered as the deepest branch within Fornicata (i.e. *Carpediemonas* was more closely related to diplomonads and retortamonads). The poor resolution of the tree of Fornicata based on SSU rRNA gene sequence might be an effect of poor taxon sampling in deep lineages, and/or variable rates of sequence evolution for this gene in these taxa. We anticipate that analyses that include additional deeply branching fornicates and examine multi-gene datasets will be required to resolve the deep relationships among Fornicata.

Taxonomic Summary

Assignment: Eukaryota; Excavata; Fornicata

Hicanonectes n. g.

Diagnosis. Free-living, biflagellated, and colourless cells bearing a longitudinal groove with a sharply defined right wall. The posterior flagellum beats within the groove, and bears vanes. The posterior end of the groove forms a curved cytopharynx. Mitochondrion-like organelles lack cristae. The anterior microtubular root is well developed and directed laterally and anteriorly (rather than curving to be directed leftwards and posteriorly). The cell rotates rapidly while swimming.

Type species. *Hicanonectes teleskopos* Park, Kolisko, Heiss & Simpson

Etymology. *Hicanonectes* = ''adequate swimmer'' (Greek; masculine). This organism is a more conventional and effective swimmer than its most similar relatives, *Carpediemonas* and *Dysnectes* (the latter name meaning ''bad swimmer''—Yubuki et al. 2007). It is, however, of only moderate abilities when compared with many flagellates from other taxonomic groups.

Hicanonectes teleskopos n. sp.

Diagnosis. Cells oval-shaped and 6.5–10.0 μm long. The posterior flagellum is 2.5–3.5 times as long as the cell; the anterior flagellum is directed sharply leftwards and is 1.0–1.5 times as long as the cell.

Type material. Block of resin-embedded cells for electron microscopy deposited with the Protist Type Specimen Slide Collection, U.S. Natural History Museum, Washington, DC, as USNM 1122785. This material constitutes the name-bearing hapantotype for the species.

Type locality. Anoxic layer of intertidal sediment, Salt Spring Island, BC, Canada (48°46′N and 123°28′W).

Etymology. *teleskopos* = ''Far see-er'' (Greek), recognizes the Canadian Institute for Advanced Research (CIfAR, pronounced ''see-far'') for long-standing support of microbial evolution research in Canada, and commemorates the isolation of this species immediately after the first full meeting of the CIfAR Program in Integrated Microbial Biodiversity, in October 2007.

ACKNOWLEDGMENTS

Thanks to David Walsh (University of British Columbia) for sampling assistance, Zhiyuan Lu (Dalhousie University) for assistance with high-pressure freezing fixation, and Harold Tarrant (Newcastle University, Australia) for advice on ancient Greek. This work is supported by NSERC grant 298366-04 to AGBS, and the Canadian Institute for Advanced Research (CIfAR) Program in Integrated Microbial Biodiversity. J.S.P. is partly supported by a Korea Research Foundation Grant funded by the Korean Government (MOEHRD, No. KRF-2007-357-C00119). M.K. is supported by the Nova Scotia Health Research Foundation. A.A.H. is partly supported by a Dalhousie University graduate student scholarship.

LITERATURE CITED

Altschul, S. F., Gish, W., Miller, W., Myers, E. W. & Lipman, D. J. 1990. Basic local alignment search tool. *J. Mol. Biol.*, **215**:403–410.

Benchimol, M. 2008. Structure of the hydrogenosome. *In*: Tachezy, J. (ed.), Hydrogenosomes and Mitosomes: Mitochondria of Anaerobic Eukaryotes. Springer-Verlag, Berlin. p. 75–97.

Bernard, C., Simpson, A. G. B. & Patterson, D. J. 1997. An ultrastructural study of a free-living retortamonad, *Chilomastix cuspidata* (Larsen and Patterson, 1990) n. comb. (Retortamonadida, Protista). *Eur. J. Protistol.*, **33**:254–265.

Brugerolle, G. 1973. Etude ultrastucturale du trophozoite du kyste chez le genre *Chilomastix* Aléxéieff, 1910 (Zoomastigophorea, Retortamonadida Grassé, 1952). *J. Protozool.*, **20**:574–585.

Brugerolle, G. 1977. Ultrastructure du genre *Retortamonas* Grassi 1879 (Zoomastigophorea, Retortamonadida Wenrich 1931). *Protistologica*, **13**:233–240.

Brugerolle, G. & Patterson, D. J. 1997. Ultrastructure of *Trimastix convexa* Hollande, an amitochondriate anaerobic flagellate with a previously undescribed organisation. *Eur. J. Protistol.*, **33**:121–130.

Carpenter, K. J., Waller, R. F. & Keeling, P. J. 2008. Surface morphology of *Saccinobaculus* (Oxymonadida): implications for character evolution and function in oxymonads. *Protist*, **159**:209–221.

Cavalier-Smith, T. 1995. Cell cycles, diplokaryosis and the archezoan origin of sex. *Arch. Protistenkd.*, **145**:189–207.

Cepicka, I., Kostka, M., Uzlikova, M., Kulda, J. & Flegr, J. 2008. Non-monophyly of Retortamonadida and high genetic diversity of the genus *Chilomastix* suggested by analysis of SSU rDNA. *Mol. Phylogenet. Evol.*, **48**:770–775.

Ciccarelli, D. F., Doerks, T., von Mering, C., Creevey, C. J., Snel, B. & Bork, P. 2006. Toward automatic reconstruction of a highly resolved tree of life. *Science*, **311**:1283–1287.

Clark, C. G. 1992. DNA purification from polysaccharide-rich cells. *In*: Lee, J. J. & Soldo, A. T. (eds.), Protocols in Protozoology. Allen Press, Lawrence, KS. **1**:D-3.1–D-3.2.

Dacks, J. B., Silberman, J. D., Simpson, A. G. B., Moryia, S., Kudo, T., Ohkuma, M. & Redfield, R. J. 2001. Oxymonads are closely related to the excavate taxon *Trimastix*. *Mol. Biol. Evol.*, **18**:1034–1044.

Diamond, L. S. 1982. A new liquid medium for xenic cultivation of *Entamoeba histolytica* and other lumen-dwelling protozoa. *J. Parasitol.*, **68**:958–959.

Ekebom, J., Patterson, D. J. & Vørs, N. 1996. Heterotrophic flagellates from coral reef sediments (Great Barrier Reef, Australia). *Arch. Protistenkd.*, **146**:251–272.

Hall, T. A. 1999. BioEdit: a user-friendly biological sequence alignment editor and analysis program for Windows 95/98/NT. *Nucl. Acids Symp. Ser.*, **41**:95–98.

Hampl, V. & Simpson, A. G. B. 2008. Possible mitochondria-related organelles in poorly-studied ''amitochondriate'' eukaryotes. *In*: Tachezy, J. (ed.), Hydrogenosomes and Mitosomes: Mitochondria of Anaerobic Eukaryotes. Springer-Verlag, Berlin. p. 265–283.

Hampl, V., Silberman, J. D., Stechmann, A., Diaz-Triviño, S., Johnson, P. J. & Roger, A. J. 2008. Genetic evidence for a mitochondriate ancestry in the 'amitochondriate' flagellate *Trimastix pyriformis*. *PLoS ONE*, **3**, e1383.

Hashimoto, T., Nakamura, Y., Kamaishi, T., Nakamura, F., Adachi, J., Okamoto, K-I. & Hasegawa, M. 1995. Phylogenetic place of mitochondrion-lacking protozoan, *Giardia lamblia*, inferred from amino acid sequences of elongation factor 2. *Mol. Biol. Evol.*, **12**:782–793.

Hashimoto, T., Nakamura, Y., Nakamura, F., Shirakura, T., Adachi, J., Goto, N., Okamoto, K-I. & Hasegawa, M. 1994. Protein phylogeny gives a robust estimation for early divergences of eukaryotes: phylogenetic place of a mitochondria-lacking protozoan, *Giardia lamblia*. *Mol. Biol. Evol.*, **11**:65–71.

Horner, D. S. & Embley, T. M. 2001. Chaperonin 60 phylogeny provides further evidence for secondary loss of mitochondria among putative early-branching eukaryotes. *Mol. Biol. Evol.*, **18**:1970–1975.

Huelsenbeck, J. P. 2000. MrBayes: Bayesian inference of phylogeny. Distributed by the author. Department of Biology, University of Rochester.

Katoh, K., Kuma, K., Toh, H. & Miyata, T. 2005. MAFFT version 5: improvement in accuracy of multiple sequence alignment. *Nucleic Acid Res.*, **33**:511–518.

Keeling, P. J. & Brugerolle, G. 2006. Evidence from SSU rRNA phylogeny that *Octomitus* is a sister lineage of *Giardia*. *Protist*, **157**:205–212.

Kolisko, M., Cepicka, I., Hampl, V., Kulda, J. & Flegr, J. 2005. The phylogenetic position of enteromonads: a challenge for the present models of diplomonad evolution. *Int. J. Syst. Evol. Microbiol.*, **55**:1729–1733.

Kolisko, M., Cepicka, I., Hampl, V., Leigh, J., Roger, A. J., Kulda, J., Simpson, A. G. B. & Flegr, J. 2008. Molecular phylogeny of diplomonads and enteromonads based on SSU rRNA, α-tubulin and HSP90 genes: implications for the evolutionary history of the double karyomastigont of diplomonads. *BMC. Evol. Biol.*, **8**:e205.

Kulda, J. & Nohýnková, E. 1978. Flagellates of the human intestine and of intestines of other species. *In*: Kreier, J. P. (ed.), Parasitic Protozoa: Volume II: Intestinal Flagellates, Histomonads, Trichomonads, Amoeba, Opalinids, and Ciliates. Academic Press, San Diego. p. 1–128.

Lara, E., Chatzinotas, A. & Simpson, A. G. B. 2006. *Andalucia* (n. gen.) – The deepest branch within jakobids (Jakobida, Excavata), based on morphological and molecular study of a new flagellate from soil. *J. Eukaryot. Microbiol.*, **53**:112–120.

Lee, W. J. & Patterson, D. J. 2000. Heterotrophic flagellates (Protista) from marine sediments of Botany Bay, Australia. *J. Nat. Hist.*, **34**:483–562.

Medlin, L., Elwood, H. J., Stickel, S. & Sogin, M. L. 1988. The characterization of enzymatically amplified eukaryotic 16S-like rRNA-coding regions. *Gene*, **71**:491–499.

O'Kelly, C. J. 1993. The jakobid flagellates: structural features of *Jakoba*, *Reclinomonas* and *Histiona* and implications for the early diversification of eukaryotes. *J. Eukaryot. Microbiol.*, **40**:627–636.

O'Kelly, C. J. 1997. Ultrastructure of trophozoites, zoospores and cysts of *Reclinomonas americana* Flavin & Nerad, 1993 (Protista *incertae sedis*: Histionidae). *Eur. J. Protistol.*, **33**:337–348.

O'Kelly, C. J. & Nerad, T. A. 1999. *Malawimonas jakobiformis* n. gen., n. sp. (Malawimonadidae n. fam.): a *Jakoba*-like heterotrophic nanoflagellate with discoidal mitochondrial cristae. *J. Eukaryot. Microbiol.*, **46**:522–531.

O'Kelly, C. J., Farmer, M. A. & Nerad, T. A. 1999. Ultrastructure of *Trimastix pyriformis* (Klebs) Bernard et al.: similarities of *Trimastix* species with retortamonad and jakobid flagellates. *Protist*, **150**:149–162.

Patterson, D. J. 1990. *Jakoba libera* (Ruinen, 1938), a heterotrophic flagellate from deep ocean sediments. *J. Mar. Biol. Assoc. UK*, **70**:381–393.

Posada, D. & Crandall, C. A. 1998. MODELTEST: testing the model of DNA substitution. *Bioinformatics*, **14**:817–818.

Rodriguez-Ezpeleta, N., Brinkman, H., Burger, G., Roger, A. J., Gray, M. W. & Lang, B. F. 2007. Toward resolving the eukaryotic tree: the phylogenetic position of jakobids and cercozoans. *Curr. Biol.*, **17**:1420–1425.

Roger, A. J., Svärd, S. G., Tovar, J., Clark, C. G., Smith, M. W., Gillin, F. D. & Sogin, M. L. 1998. A mitochondrial-like chaperonin 60 gene in *Giardia lamblia*: evidence that diplomonads once harboured an endosymbiont related to the progenitor of mitochondria. *Proc. Natl. Acad. Sci. USA*, **95**:229–234.

Simpson, A. G. B. 2003. Cytoskeletal organisation phylogenetic affinities and systematics in the contentious taxon Excavata (Eukaryota). *Int. J. Syst. Evol. Microbiol.*, **53**:1759–1777.

Simpson, A. G. B. & Patterson, D. J. 1999. The ultrastructure of *Carpediemonas membranifera* (Eukaryota) with reference to the ''excavate hypothesis''. *Eur. J. Protistol.*, **35**:353–370.

Simpson, A. G. B. & Patterson, D. J. 2001. On core jakobids and excavate taxa: the ultrastructure of *Jakoba incarcerata*. *J. Eukaryot. Microbiol.*, **48**:480–492.

Simpson, A. G. B., Bernard, C. & Patterson, D. J. 2000. The ultrastructure of *Trimastix marina* Kent 1880 (Eukaryota), an excavate flagellate. *Eur. J. Protistol.*, **36**:229–252.

Simpson, A. G. B., Inagaki, Y. & Roger, A. J. 2006. Comprehensive multigene phylogenies of excavate protists reveal the evolutionary position of ''primitive'' eukaryotes. *Mol. Biol. Evol.*, **23**:615–625.

Simpson, A. G. B., MacQuarrie, E. K. & Roger, A. J. 2002a. Eukaryotic evolution: early origin of canonical introns. *Nature*, **419**:270.

Simpson, A. G. B., Roger, A. J., Silberman, J. D., Leipe, D. D., Edgcomb, V. P., Jermiin, L. S., Patterson, D. J. & Sogin, M. L. 2002b. Evolutionary history of ''early diverging'' eukaryotes: the excavate taxon *Carpediemonas* is a close relative of *Giardia*. *Mol. Biol. Evol.*, **19**: 1782–1791.

Sleigh, M. A. 1988. Flagellar root maps allow speculative comparisons of root patterns and of their ontogeny. *BioSystems*, **21**:277–282.

Sogin, M. L., Gunderson, J. H., Elwood, H. J., Alonso, R. A. & Peattie, D. A. 1989. Phylogenetic meaning of the kingdom concept: an unusual ribosomal RNA from *Giardia lamblia*. *Science*, **243**:75–77.

Swofford, D. L. 2003. PAUP: Phylogenetic Analyses Using Parsimony (*and other Methods). Sinauer Associates, Sunderland, MA.

Tachezy, J., Sánchez, L. B. & Müller, M. 2001. Mitochondrial type iron–sulfur cluster assembly in the amitochondriate eukaryotes *Trichomonas vaginalis* and *Giardia intestinalis*, as indicated by the phylogeny of IscS. *Mol. Biol. Evol.*, **18**:1919–1928.

Takishita, K., Yubuki, N., Kakizoe, N., Inagaki, Y. & Maruyama, T. 2007. Diversity of microbial eukaryotes in sediment at a deep-sea methane cold seep: surveys of ribosomal DNA libraries from raw sediment samples and two enrichment cultures. *Extremophiles*, **11**:563–576.

Thompson, J. D., Gibson, T. J., Plewniak, F., Jeanmougin, F. & Higgins, D. G. 1997. The ClustalX windows interface: flexible strategies for multiple sequence alignment aided by quality analysis tools. *Nucleic Acids Res.*, **24**:4876–4882.

Tovar, J., León-Avilla, G., Sánchez, L. B., Sutak, R., Tachezy, J., van der Giezen, M., Hernandez, M., Müller, M. & Lucocq, J. M. 2003. Mitochondrial remnant organelles of *Giardia* function in iron–sulfur protein maturation. *Nature*, **426**:172–176.

Vinh, L. S. & von Haeseler, A. 2004. IQPNNI: moving fast through tree space and stopping in time. *Mol. Biol. Evol.*, **8**:1565–1571.

Yubuki, N., Inagaki, Y., Nakayama, T. & Inouye, I. 2007. Ultrastructure and ribosomal RNA phylogeny of the free-living heterotrophic flagellate *Dysnectes brevis* n. gen, n. sp., a new member of Fornicata. *J. Eukaryot. Microbiol.*, **54**:191–200.

Received: 11/05/08, 02/27/09; accepted: 03/03/09